Journal of Luminescence 230 (2021) 117639

Contents lists available at ScienceDirect

Journal of Luminescence

journal homepage: http://www.elsevier.com/locate/jlumin

Determination of the refractive index of $BaY_2F_8:Er^{3+}$ (0.5 mol% to 30 mol %) in the 300 nm–1800 nm range by ellipsometry; a record-breaking upconversion material

Joseph Gibbons [a], Callum M.S. Jones [a], Nick S. Bennett [b], Jose Marques-Hueso [a,*]

[a] Institute of Sensors, Signals and Systems, School of Engineering & Physical Sciences, Heriot-Watt University, Edinburgh, EH14 4AS, Scotland, UK
[b] Faculty of Engineering and Information Technology, University of Technology Sydney, PO Box 123, Broadway, NSW, 2007, Australia

ARTICLE INFO

Keywords:
Barium yttrium fluoride
Refractive index
Spectroscopic ellipsometry
Upconversion material

ABSTRACT

This work reports the ellipsometric study of trivalent erbium (Er^{3+}) doped monocrystalline barium yttrium fluoride (BaY_2F_8), which has recently been shown to be one of the best photon upconversion (UC) materials available. This spans the BaY_2F_8 applications in a large range of wavelengths, from ultraviolet (UV) to near-infrared (NIR). We detail the optical properties of BaY_2F_8: Er^{3+} (0.5 mol%, 10 mol%, and 30 mol%), measured via variable angle spectroscopic ellipsometry over a spectral range from 300 nm to 1800 nm, reporting for the first time the indices of refraction for $BaY_2F_8:Er^{3+}$. The upconversion external photoluminescence quantum yield (*e*PLQY) of the $BaY_2F_8:Er^{3+}$ samples have also been studied by exciting at $[JG]\lambda = 1588\ nm\ \lambda =$ 1493 nm. The highest *e*PLQY of BaY_2F_8 was found for the largest dopant concentration 30 mol% Er^{3+} reaching the value of [JG]1.07% ± 0.12%, at an irradiance of $9.512 \times 10^{-2} W/cm^2$3.62% ± 0.01%, at an irradiance of $(6.23 \pm 0.45) \times 10^{-2}$ W/cm^2. The refractive index ($\lambda = 589.3$ nm) was determined to be 1.4808± 0.014 for 0.5 mol%, 1.4980± 0.003 for 10 mol%, and 1.5022± 0.006 for 30 mol%. Increasing Er^{3+} doping concentration increased the refractive index. All samples decreased monotonically with increasing wavelength. The Brewster angle of $BaY_2F_8:Er^{3+}$ is observed to be ≈ 56°, whilst the Abbe number of the samples was found to be as high as 124.62. These findings provide valuable insight into the optical properties of $BaY_2F_8:Er^{3+}$ in the wide range of frequencies that is has proven useful.

1. Introduction

Fluoride compounds doped with rare-earth (RE) ions are attractive for optical applications as they exhibit low phonon energies and optical transparency over a broad spectral range [1–5]. The photoluminescence of the RE ions is influenced by the host material, which plays an important role in achieving a highly-efficient photon upconversion (UC) emission.

Barium yttrium fluoride (BaY_2F_8) presents an attractive host candidate; it has been shown to be one of the most efficient host materials for UC [6], and has favourable chemical and mechanical properties [7]. The crystal structure of BaY_2F_8 is monoclinic, with space group C_2, and the RE ions occupy the Y^{3+} sites (C_2 local point symmetry) [7–9]. Owing to its exceptional properties, RE ion-doped BaY_2F_8 has been extensively studied for its potential application as a solid-state laser host [10–12], and as prospective high-density optical media for scintillators [13–16].

UC is an anti-Stokes type optical emission process which exhibits a non-linear power dependency [17], where long wavelength radiation is converted to a shorter wavelength via a two or multi photon mechanism [17–21]. UC materials have received increasing attention in recent years for a huge variety of applications, for example, in microscopy and multimodal *in vivo* imaging [22,23], medical photodynamic therapy for cancer treatment [24], theranostics [25,26], dye lasers [27], optical thermometry [28], thermal sensors [29,30], and for the enhancement of photovoltaic (PV) devices [19,21]. This last application makes use of a large range of wavelengths, and requires high photoluminescence quantum yields (PLQY) at low irradiance. The PLQY is independent of instrument settings, and is therefore an important *figure-of-merit* for comparing the efficiency of the UC mechanism or the performance of UC materials, and evaluating UC enhancement techniques.

Hexagonal sodium yttrium fluoride (β-$NaYF_4$) doped with trivalent erbium (Er^{3+}) has been a usual choice due to its relatively wide

* Corresponding author.
E-mail address: J.Marques@hw.ac.uk (J. Marques-Hueso).

https://doi.org/10.1016/j.jlumin.2020.117639
Received 6 July 2020; Received in revised form 4 September 2020; Accepted 7 September 2020
Available online 20 October 2020

absorption and UC excitation spectra [31–35]. Ivaturi et al. [35] investigated the infrared ($\lambda = 1523$ nm) to near-infrared ($\lambda =$ 980 nm) PLQY of β-$NaYF_4$:Er^{3+} embedded in a perfluorocylobutane (PFCB) polymer host matrix. The best performance was determined for 25 mol% Er^{3+} with an external PLQY (*e*PLQY) of 6.5% ± 0.7% at an irradiance of $(0.097 \pm 0.004) \times 10^{-2}$ W/cm^2. PFCB was chosen as the host matrix due to its transparency at near-infrared (NIR) and having a matching refractive index of β-$NaYF_4$:25 mol% Er^{3+} [32,36].

It has been shown that monocrystalline BaY_2F_8 doped with Er^{3+} can achieve even greater *e*PLQY [37,38], with best performance determined for 30 mol% Er^{3+} with an *e*PLQY of 9.5% ± 0.7% at an irradiance of [JG] $(0.47 \pm 0.03) \times 10^{-2}$ W/$cm^2$4740 W/m^2 (or 47.40 × 10^{-2} W/cm^2), achieved due to the high absorption coefficient of the UC material [38]. Due to the strong absorption, high [JG]external*e*PLQY, broad spectrum, and stability of BaY_2F_8:Er^{3+}, it is an ideal UC material and has been used to obtain a NIR UC record efficiency in PV devices [39,40].

Due to the non-linear power dependency of UC and the influence a refractive index mismatch between the surrounding material and the fluoride crystals doped with RE ions has on scattering, and therefore the UC process efficiency [41,42]; the suitably of BaY_2F_8 for lanthanide doping and optical applications in a large range of the ultraviolet (UV) to NIR spectrum stipulates the accurate determination of the dispersion of the refractive index necessary, however, it is still not explored in the literature.

To the best of our knowledge, this paper describes for the first time the spectral index of refraction (n) in the 300 nm–1800 nm range, the extinction coefficient (k), the Brewster angle (θ_B), and the Abbe number (ν_D) of BaY_2F_8, measured for three different Er^{3+} doping concentrations (0.5 mol%, 10 mol%, and 30 mol%).

2. Experimental and analytical techniques

2.1. Crystal synthesis

BaY_2F_8 single crystal samples, doped with Er^{3+}, were developed by Mega Materials s.r.l-Pisa-Italy. The crystals were grown by the Czochralski method in a custom-built furnace as presented previously in Refs. [37]. To avoid contamination, growth fluoride powders with a purity of 99.999% (5 N) were used, and the furnace evacuated to pressures below 10^{-7} mbar before the growth process. [JG]The powders placed in the crucible were measured with 10^{-3} g precision. Typical crystal weight is 10 g. This translates to a precision of ± 0.01% in weight. During growth, the rotation rate of each sample was 5 rpm, the pulling rate 0.5 mm/h, and the temperature of the melt approximately 1200 K. The rods were cut by a diamond saw synthesis. [JG]Fourier transform infrared spectroscopy (FT-IR) analysis (Thermo Scientific Nicolet iS 5 FTIR Spectrometer) was conducted to detect hydroxide (OH) impurity within the samples. However, we were unable to detect a peak in any of the samples at 3621 cm^{-1}; a wavenumber where OH peaks [43]. [JG]More information about the synthesis of the crystals can be obtained from Ref. [37].

The diameter of the 0.5 mol% and 10 mol% Er^{3+} samples was (4 ± 0.229) mm; and for 30 mol% Er^{3+}, (10 ± 0.229) mm. The thickness of all the prepared samples was (2 ± 0.229) mm.

2.2. Sample preparation

To avoid non-specular scattering of the incident beam and depolarization of the specularly reflected beam during ellipsometric measurements, the surface of each BaY_2F_8:Er^{3+} sample was lapped (via a wet process) using an optical fibre polisher (Buehler FibrMet) to ensure surface roughness features, that is, the arithmetic average roughness (R_a), were less than 10% of the probe beam wavelength. This was firstly done using a 9 m grade aluminium oxide (Al_2O_3) abrasive lapping film disc, then a 1 μm grade Al_2O_3 disc.

As each sample is semi-transparent, and considered 'optically thick' (i.e., > 0.1 mm thick), the rear surface of each sample was roughened to avoid a second beam mixing coherently with the first and the partially polarized beam entering the detector.

An optical phase-shifting interferometer (ZYGO ZeGage Pro) was used to examine and quantify the surface roughness, step heights, and other topographical features of the BaY_2F_8:Er^{3+} substrates. [JG]The instrument employs a high resolution 1.9-million-pixel image sensor, with measurement results being ISO 25178-compliant. The instrument model is known to exhibit excellent agreement with precise contact stylus metrology measurements on reference specimens standardised in ISO 5436 Part 1:2000 [44].

2.3. Photoluminescent quantum yield

The *e*PLQY quantifies the emission efficiency of the media or sample as a whole, and is therefore defined as the ratio of the number of emitted photons (φ_{UC}) to the number of incident photons (φ_{in}) (Eq. (1)):

$$ePLQY = \frac{\varphi_{UC}}{\varphi_{in}} \tag{1}$$

The *e*PLQY measurements where performed on the BaY_2F_8: Er^{3+} single crystals using a calibrated spectrofluorometer (Edinburgh Instruments, FLS920) equipped with an integrating sphere (Jobin-Yvon), using a 6 W super-continuum (SC) laser (Fianium) as the excitation source, and a liquid-nitrogen cooled NIR photon multiplier tube (PMT; Hamamatsu, R-5587).

The excitation intensity was measured with the sample in the chamber and also with the sample absent from the chamber, with the total number of observed incident photons determined, and ultimately used to calculated the *e*PLQY.

The excitation focused beam size was measured using the 20/80 knife-edge scan technique [45,46]; and was determined to have a spot diameter beam area of [JG](8.726 ± 0.5) × 10^{-3} cm^2 (6.74 ± 0.47) × $10^{-2}cm^2$. A maximum power of [JG](0.83 ± 0.2) mW (4.19 ± 0.02) mW was achievable at the chosen wavelength from the SC laser, resulting in a power density of [JG]9.512 × 10^{-2} W/cm^2(6.23 ± 0.45) × 10^{-2} W/cm^2.

2.4. Spectroscopic ellipsometry and analysis

Variable-angle spectroscopic ellipsometry (VASE) measurements were performed (J.A. Woollam Base VASE) over a spectral range of 300 nm–1800 nm. The spectroscopic scan measures the change in polarization state of light reflected from the surface of a sample. The instrument employs a rotating analyzer, with an AutoRetarder that modifies the light beam polarization before it reaches the sample. This confers high accuracy to the technique, and relative errors lower than 0.2% can be achieved [47,48]. A stacked solid-state photodiode detector unit is used, consisting of silicon (Si) and indium gallium arsenide (InGaAs) detectors which provide a continuously measurable spectral range.

Spectroscopic ellipsometric measurements were conducted using light incident angles of 65° to 75°, at 5° increments, relative to normal on the front surface of the sample. These angles were selected as the delta data for these three angles of incidence where close to Δ = 0° or Δ = 180°, which, for an optically thick bulk sample are considered satisfactory [49–51].

The instrument measures the ellipsometric parameters expressed as psi (ψ, the amplitude component) and delta (Δ, the phase difference), based on the assumption that the sample Jones matrix is diagonal, and are defined [52] as (Eq. (2)):

$$\rho = \frac{R_p}{R_s} = tan(\psi)e^{i\Delta} \tag{2}$$

where R_p/R_s is the complex ratio of the $p-$ and $s-$ polarized light

components of the reflected amplitudes. These are analysed using the Fresnel equations [49] in a computer-based modelling technique, including an optical layer model to directly determine the optical constants [53]. The polarizer azimuth was tracked to the ψ value being measured, thus, minimizing errors.

The ellipsometry data, taken from the sample substrate, was fit, in a non-linear regression sense, to an optical model to determine complex refractive index [50] (Eq. (3)):

$$\hat{n} = n + ik \tag{3}$$

The Abbe number (ν_D) of each BaY_2F_8:Er^{3+} sample has been determined, quantifying the mean and partial refractive index (n) dispersion, over the spectral range, for the ellipsometric analysis, and is defined [54–56] as (Eq. (4)):

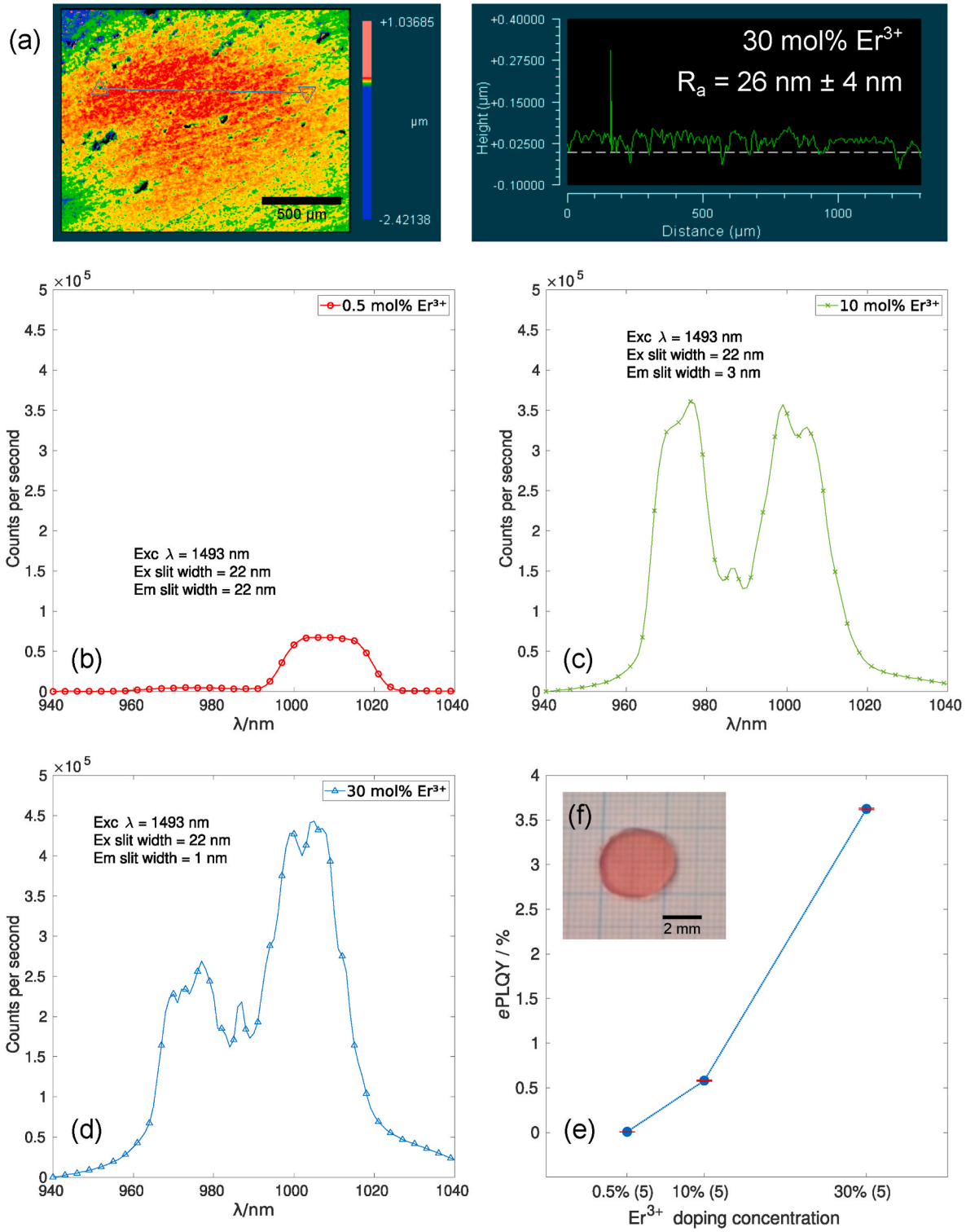

Fig. 1. **(a)** Interferogram (left) and the corresponding surface wavefront profile (right) of the BaY_2F_8: 30 mol% Er^{3+} sample; **(b–d)** Upconversion photoluminescence spectra of each sample, as annotated, detailing the number of events for the samples measured under λ = 1493 nm excitation and power density of (6.23 ± 0.45) × 10^{-2} W/cm^2; **(e)** Mean (± S.D.) *e*PLQY of the samples measured; and **(f, insert)** Photograph of the 30 mol% Er^{3+} sample.

$$\nu_D = \frac{n_D - 1}{n_F - n_C} \tag{4}$$

where n_D, n_F, and n_C are the refractive indices of the material at the wavelengths of the sodium D ($\lambda = 589.3$ nm), hydrogen F ($\lambda = 486.1$ nm), and hydrogen C ($\lambda = 656.3$ nm) lines, respectively.

The (complex) Brewster angle (θ_B), or the polarization angle, of each sample at which reflection coefficient for *p*-polarization (r_P) = 0, has been calculated, which provides maximal sensitivity to the properties of the sample, and is defined [57,58] as (Eq. (5)):

$$\theta_B = \arctan\left(\frac{n_2}{n_1}\right) \tag{5}$$

where n_1 is the refractive index of the initial medium through which light propagates (the 'incident medium'); and n_2 is the measured refractive index of the other medium. Note: r_P is defined [57,58] as (Eq. (6)):

$$r_p = \frac{n_2\cos\theta_{incident} - n_1\cos\theta_{transmitted}}{n_1\cos\theta_{transmitted} + n_2\cos\theta_{incident}} \tag{6}$$

where $\theta_{incident}$ and $\theta_{transmitted}$ are the angles of incidence and transmittance upon a medium.

3. Results and discussion

The interferogram measurements, and corresponding surface wavefront profiles for selected region, obtained from the optical phase-shifting interferometer are shown (Fig. 1a). Each sample was lapped and intermittently examined with the interferometer until the arithmetic average roughness (R_a) was determined to be within an acceptable limit. Result shown is the final surface roughness measurement obtained. The 10% and 30% Er^{3+} samples where lapped to an R_a of < 30 nm (i.e., less than 10% of the shortest probe beam wavelength), and the 0.5% Er^{3+} sample was lapped to [JG]an [JG]a mean R_a of [JG]36.287 nm36 nm ± 4 nm.

The obtained photoluminescence spectra, and the determined *e*PLQY of the BaY_2F_8 samples for the corresponding Er^{3+} doping concentrations, measured under [JG]$\lambda = 1588$ nm$\lambda = 1493$ nm excitation, are compared (Fig. 1b [JG]and to Fig. 1[JG]ce). [JG]It is generally more common to measure the PLQY for the transition $^4I_{11/2} \rightarrow {}^4I_{15/2}$ (in the 980 nm range), as this accounts for approximately 97% of UC emission [59], and including higher photon emission in the calculation would increase PLQY only fractionally. However, the *e*PLQY of the BaY_2F_8 sample with 0.5% Er^{3+} doping needed different excitation slits (and therefore, a different excitation wavelength) to get a measurable emission. Furthermore, the measured emission signal of the 0.5% Er^{3+} doped BaY_2F_8 sample, with excitation wavelength of $\lambda = 1520$ nm, was low enough for a double excitation wavelength to be detected, caused by secondary order effects. Thus, all samples where measured with an excitation of $\lambda = 1588$ nm to allow comparable results to be produced All samples where measured with an excitation of $\lambda =$ 1493 nm, an excitation slit width of 22 nm, and with an approximately constant power density of (6.23 ± 0.45) × 10^{-2} W/cm^2 to allow comparable results to be produced. The excitation wavelength $\lambda =$ 1493 nm was selected as the absorption coefficient of BaY_2F_8:Er^{3+} is known to reach its highest peak centred at 1493 nm [37,60]. The area underneath each spectrum represents the total number of emitted photons between [JG]920 nm940 nm and [JG]1060 nm1040 nm which is directly proportional to the *e*PLQY of the samples. [JG]The emission slit widths changed between measurements to protect the detector and were: 22 nm for the 0.5 mol% Er^{3+} sample; 3 nm for the 10 mol% Er^{3+} sample: and 1 nm for the 30 mol% Er^{3+} sample. As a result, although the *e*PLQY results of each sample are directly comparable with each other, the resolution and intensity of the spectra peaks obtained aren't. [JG]The 10 mol%, and 30 mol % Er^{3+} doping levels present a similar distribution: the highest peak centred at 1002 nm, with a second peak at 978 nm. The 0.5 mol% Er^{3+} doped sample, however, only presents a single peak, at 972 nm. As anticipated, the *e*PLQY changes drastically within different Er^{3+} doping concentrations, with the absolute highest *e*PLQY value observed for the BaY_2F_8: 30% Er^{3+} sample reaching the value of [JG]1.07% ± 0.12%3.62% ± 0.01%. The doping concentration of Er^{3+} significantly impacts the UC emission process, and therefore the *e*PLQY. This is due to the *concentration quenching mechanism*; whereby high doping levels may result in the quenching of excitation energy, whereas low doping levels may result in low absorption of the incident light [61].

The photoluminescence findings of the current study are consistent with those of Boccolini et al. [37] and Fischer et al. [38] who found that 30 mol% Er^{3+} doped BaY_2F_8 samples yielded best *e*PLQY performance. We obtained an *e*PLQY [JG] = 1.07% ± 0.12%of = 3.62% ± 0.01% [JG] because the maximum irradiance was as low as 9.512 × 10^{-2}W/cm^2at an irradiance of (6.23 ± 0.45) × 10^{-2} W/cm^2 under illumination at $\lambda =$ 1493 nm, while Fischer et al. [JG]obtained an *e*PLQY = 9.50% ± 0.70%, measured with a more optimal UC energy transfer probability excitation $\lambda =$ 1520 nm, and a maximum irradiance as high as 47.40 × 10^{-2} W/cm^2.measured a *e*PLQY of ≈ 3.6% at an irradiance of ≈ 6.5 × 10^{-2} W/cm^2 under illumination at $\lambda = 1520$ nm.

For the ellipsometric measurements, the experimental Delta (Δ) data for angle of incidence of 65°, 70°, and 75° where found to generally distribute Δ ≈ 0° for all three samples [49]. States that Δ, that is, the phase shift (difference), should always be either 0° (for angles of incident greater than the θ_B) or 180° (for angles of incidence less than the θ_B) for a transparent bulk sample, as the light beam entering the detector will always be linearly polarized. A bulk sample here is considered to be an optically thick substrate with no coatings or multilayer on its surface. The experimental and calculated data of each sample was compared; with the experimental-versus-modelled difference of the ψ, that is, the amplitude component, for each sample reviewed (Fig. 2) and found to distribute around 0.

Two optical layer models where assessed to determine best fit: *(a)* a single isotropic Cauchy optical constants function based layer [62]; and *(b)* a generalized oscillating Sellmeier optical layer [63]. These models

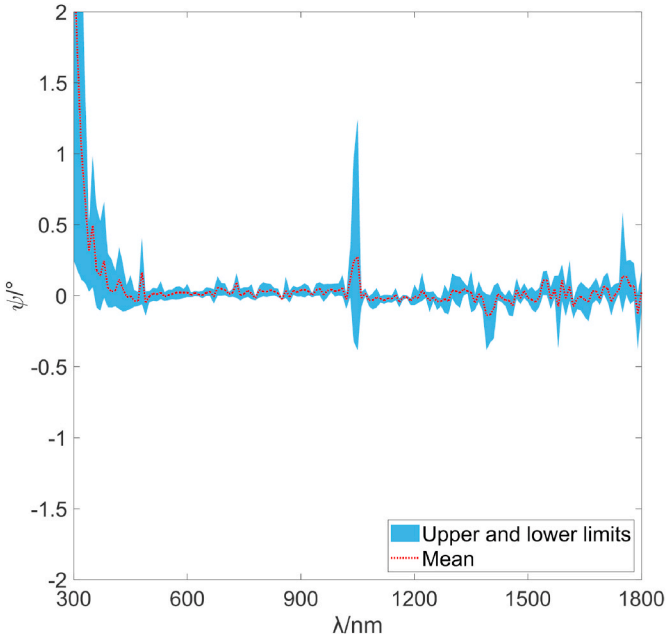

Fig. 2. The upper limit, lower limit, and the mean difference between the combined calculated and experimental ψ data for all samples over the spectral range. The values show dominant errors which are approximately random and, with the exception of $\lambda \approx 1000$ nm, caused by the Si → InGaAs detector change, and < 400 nm which shows greater error, are distributed around zero.

are typical for the parametrization of the index of transparent or semi-transparent materials. Neither method insists on Kramers-Kronig consistency.

The Cauchy function describes the dispersion over part of the spectral range, and fits the optical constants using the iterative Levenberg-Marquardt fitting algorithm [64,65]. The index of refraction (n), and extinction coefficient (k), are represented by a slowly varying function of wavelength (λ), and an exponential absorption tail [49,66]. Initial values for layer thickness (1 mm) and A_n (1.45) were selected to simulate the interaction of polarized light with the sample and generate data.

The generalized oscillating Sellmeier optical layer fits the optical constants on a normal basis over the full spectral range. The Sellmeier and Pole oscillator terms describe zero broadening oscillators, thus, the model is only fit to the real part of the dielectric function (ε_1) spectrum, since the imaginary part of the dielectric function is zero (i.e., $2 = 0$) [49,51].

The mean-squared error (MSE) is used as the maximum likelihood estimator, defined to represent the quality of the match between data calculated from the model and experimental data [49]. The Levenberg-Marquardt multi-iterative regression algorithm is employed for all model minimizations and for analysis of the calibration data to obtain calibration parameters. The model is used to calculate the adjustments to the variable parameters, at a given point on the MSE surface, as the solutions of the linear set. Convergence is reached when successive iterations are unable to improve the MSE. The resulting best-fit parameter values are evaluated for *(a)* sensitivity, expressed in terms of a confidence limit; and *(b)* possible correlations, expressed in terms of a set of two parameter correlation coefficients.

The results of the indices of refraction, modelled using the isotropic Cauchy optical constants function based layer and the two-pole general oscillating Sellmeier layer, were found to be near identical in profile. With the Cauchy layer found to be the best-fit (i.e., a lower MSE value) for all three samples.

The complex indices of refraction of each sample, over the spectral region, are shown (Fig. 3), with the index of refraction and extinction coefficient listed (Table 1). The reference wavelength $\lambda = 589.3$ nm (the sodium D line [67]) is selected for the description of the index of refraction. The index values presented show that BaY_2F_8 with 30 mol% Er^{3+} doping has the highest index of refraction of the samples studied. The index of refraction exhibits strong dispersion over the spectral range where the absorption of the material is zero, and decreases monotonically with increasing wavelength. It can be seen that the increasing Er^{3+} concentration results in a higher overall value for n.

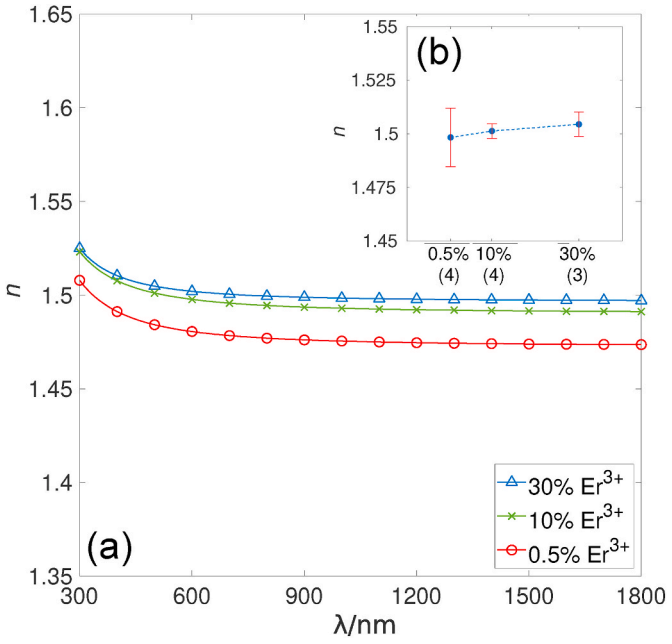

Fig. 3. (a) The ellipsometric real part of the pseudo index of refraction (n) values of the BaY_2F_8:Er^{3+} samples. Data determined by applying the Levenberg-Marquardt fitting algorithm to the ellipsometric data over the spectral range; and **(b)** Mean ($\pm$ S.D.) refractive index values (λ = 589.3 nm) of the single BaY_2F_8 crystal samples, by Er^{3+} doping concentration. Numbers in the parentheses on x-axis labels represent number of repeat measurements.

In comparison, En-Cai et al. [68] investigated the spectroscopic properties of trivalent holmium ion (Ho^{3+}) doped BaY_2F_8, and calculated a refractive index of 1.51 (λ = 589.3 nm) using a one-term Sellmeier dispersion equation with parameters from Ref. [69]. Similarly, Toncelli et al. [70] in a study of europium ion (Eu^{2+}) doped BaY_2F_8, report that the matrix has a monochromatic refractive index of around 1.5. The values of these studies agree with the ones reported here.

The high Abbe number (i.e., > 40) of each BaY_2F_8 sample (Table 1) is consistent with other material groupings, accomplished in accordance with a materials refractive index value and dispersion characteristic, whereby refractive indices < 1.55 typically have a magnitude of ν_D above 40. The large ν_D magnitudes found for the samples is representative of their low dispersion over the measured spectra.

The measured ψ and Δ parameters determined as a function of angle of incidence, between angles 15°–90°, are presented (Fig. 4). ψ approximately equals 42° (trending towards 45° as angle incidence decreases to 0°) and Δ approximately equals 180° at normal angle of incidence, which corresponds to the reflected beam exhibiting the same polarization state as that of the incident beam. As the angle of incidence increases, ψ decreases until it reaches a minimum for all three samples at about 56° angle of incidence, and is identified as the Brewster angle (Table 1). ψ does not go to 0° for any of the samples, rather its minimum value (seen for 30 mol% Er^{3+}) at the Brewster angle is 0.88°. The Δ value of the three samples does not change abruptly from 180° to 0° at the Brewster angle, rather this transition occurs over a range of angles of incidence centred on the Brewster angle. This is known to occur for bulk, bare substrates, where increasing values of the extinction coefficient lead to larger values of ψ at the Brewster angle and a broader transition region for Δ. Assuming a refractive index of 1.00027717 for air [71], and using the measured n value of BaY_2F_8: 30 mol% Er^{3+} of 1.5022; the theoretical θ_B value equates to 56.3°, showing good agreement with our measurements.

4. Conclusion

An ellipsometric study of single BaY_2F_8 crystal samples, with Er^{3+} doping concentrations of 0.5 mol%, 10 mol%, and 30 mol%, has been presented, together with the corresponding Cauchy dispersion formulae parameters, for the first time. It has been shown that, depending on the Er^{3+} doping concentration, BaY_2F_8: Er^{3+}, has a refractive index of 1.4808 $\pm$ 0.014 for 0.5 mol%, 1.4980 $\pm$ 0.003 for 10 mol%, and 1.5022 $\pm$ 0.006 for 30 mol%. The Abbe number of each sample is 90.62; for 0.5 mol%, 98.25; for 10 mol%, and for 30 mol%, 124.62. The Brewster angle of the samples, irrespective of Er^{3+} doping concentration, was observed to be 56°.

The highest *e*PLQY measured in this study was for a BaY_2F_8: 30 mol% Er^{3+} sample of thickness (2 $\pm$ 0.229) mm, reaching the value of [JG] 1.07% $\pm$ 0.12%3.62% $\pm$ 0.01%, obtained under [JG]λ = 1588 nmλ = 1493 nm excitation and with a maximum irradiance of [JG]9.512 $\times$ 10^{-2} W/cm^2(6.23 $\pm$ 0.45) $\times$ 10^{-2} W/cm^2.

The determined optical properties provide insight to aid the development of improving or optimizing the UC emission and efficiency performance of Er^{3+} doped BaY_2F_8. With the refractive indices of BaY_2F_8:Er^{3+} known, and given the influence the refractive index mismatch between host material and doped fluoride crystals has on the UC efficiency due to the scattering effects [42]; it is recommended that future work is conducted to identify an encapsulate material with

Table 1
The Cauchy parameters, derived from the Levenberg-Marquardt fitting algorithm, the MSE of the optical model, the determined index of refraction (n, $\lambda =$ 589.3 nm) and extinction coefficient (k, $\lambda = 589.3$ nm), the calculated Abbe number (ν_D), the observed θ_B, and the ePLQY of each BaY_2F_8 sample. The MSE value of each Cauchy layer fit is < 10, and is considered acceptable. A trend of increasing n and ν_D with increasing Er^{3+} concentration is observed.

Er^{3+}	Cauchy coefficients								
(mol%)	A	B	C	MSE	n ($\lambda = 589.3$ nm)	k ($\lambda = 589.3$ nm)	ν_D	θ_B (°)	ePLQY (%)
0.5	1.4272	0.0027065	$4.1133e^{-5}$	5.222	1.4808 (± 0.014)	0.0680	90.62	56	[JG]0.008 (± 0.001)
10	1.4904	0.0025155	$3.8389e^{-5}$	2.525	1.4980 (± 0.003)	0.0359	98.25	56	[JG]0.582 (± 0.006)
30	1.4966	0.0017635	$7.1446e^{-5}$	4.482	1.5022 (± 0.006)	0.0141	124.62	56	[JG]3.623 (± 0.010)

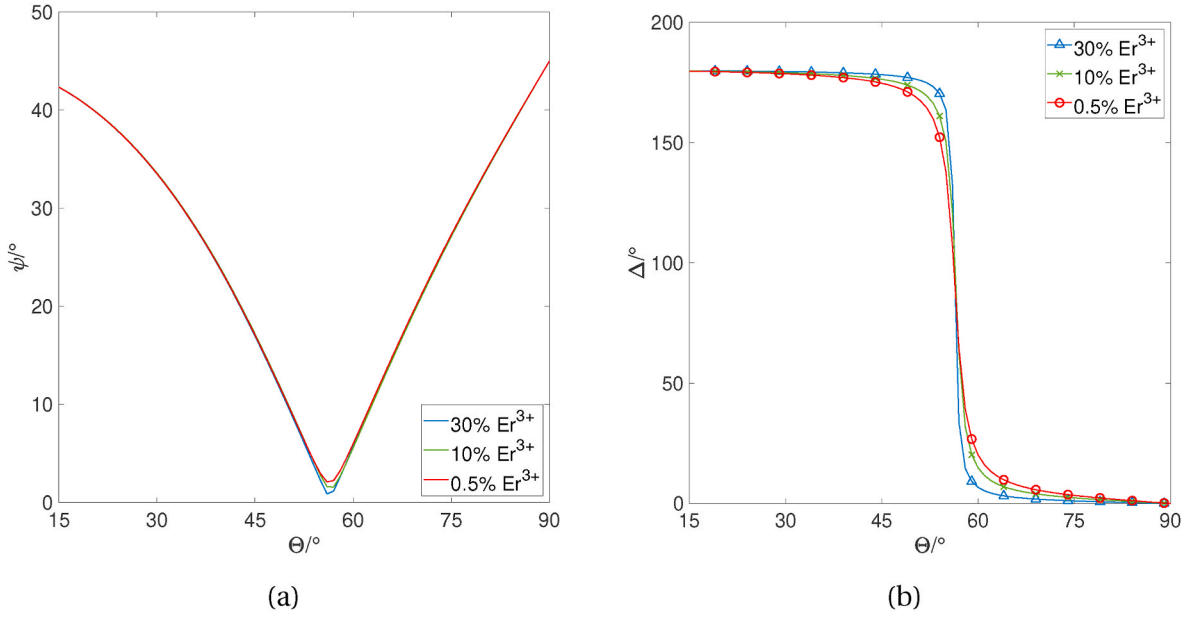

Fig. 4. The ellipsometric **(a)** Psi (ψ) and **(b)** Delta (Δ) calculated values as a function of incidence angle for the BaY_2F_8:Er^{3+} samples. Data determined by applying the Levenberg-Marquardt fitting algorithm to the ellipsometric data over angle of incidence at λ = 589.3 nm. It can be seen that the increasing Er^{3+} concentration resulted in a sharper Δ trend.

optimum refractive index properties to enhance PLQY performance when embedding BaY_2F_8:Er^{3+} into an optical device.

CRediT statement

Joseph Gibbons: Methodology, Formal analysis, Investigation, Writing - Original. Draft, and Visualization. **Callum M.S. Jones**: Methodology, and Formal analysis. **Nick S. Bennett**: Funding acquisition; and Writing - Review & Editing. **Jose. Marques-Hueso**: Conceptualization, Writing - Review & Editing, Supervision, and Funding acquisition.

Declaration of competing interest

The authors declare that they have no known competing financial interests or personal relationships that could have appeared to influence the work reported in this paper.

Acknowledgements

We thank Mark Leonard, experimental officer at Heriot-Watt University, for his assistance with the sample preparation for ellipsometric analysis.

This work was supported by the UK Engineering and Physical Sciences Research Council [grant numbers EP/R512539/1 and EP/T013680/1].

References

[1] Y.W. Zhang, X. Sun, R. Si, L.P. You, C.H. Yan, Single-crystalline and monodisperse LaF3 triangular nanoplates from a single-source precursor, J. Am. Chem. Soc. 127 (10) (2005) 3260–3261, https://doi.org/10.1021/ja042801y.

[2] J.-H. Zeng, J. Su, Z.-H. Li, R.-X. Yan, Y.-D. Li, Synthesis and upconversion luminescence of hexagonal-phase $NaYF_4$:Yb, Er3+ phosphors of controlled size and morphology, Adv. Mater. 17 (17) (2005) 2119–2123, https://doi.org/10.1002/adma.200402046.

[3] X. Wang, J. Zhuang, Q. Peng, Y. Li, Hydrothermal synthesis of rare-earth fluoride nanocrystals, Inorg. Chem. 45 (17) (2006) 6661–6665, https://doi.org/10.1021/ic051683s.

[4] L. Wang, Y. Li, Controlled synthesis and luminescence of lanthanide doped NaYF4 nanocrystals, Chem. Mater. 19 (4) (2007) 727–734, https://doi.org/10.1021/cm061887m.

[5] J.H. Zeng, T. Xie, Z.H. Li, Y. Li, Monodispersed nanocrystalline fluoroperovskite up-conversion phosphors, Cryst. Growth Des. 7 (12) (2007) 2774–2777, https://doi.org/10.1021/cg070477n.

[6] M.P. Hehlen, M.L.F. Phillips, N.J. Cockroft, H.U. Güdel, Upconversion Phosphors, second ed., 2001, https://doi.org/10.1016/B0-08-043152-6/01709-5.

[7] M. Karbowiak, A. Mech, A. Bednarkiewicz, W. Strek, Synthesis and properties of solution-processed Eu3+:BaY 2F8, J. Lumin. 114 (1) (2005) 1–8, https://doi.org/10.1016/j.jlumin.2004.11.004.

[8] N.L. Tkachenko, L.S. Garashina, O.E. Izotova, V.B. Aleksandrov, B.P. Sobolev, Phase equilibria in BaF_2(Y, Ln)F_3 systems, J. Solid State Chem. 8 (3) (1973) 213–218, https://doi.org/10.1016/0022-4596(73)90087-X.

[9] Q. Chen, X. Lai, T. Tang, B. Bai, M. Chu, Y. Zhang, S. Tan, First-principles study of the electronic structure and optical properties of UO2, J. Nucl. Mater. 401 (1–3) (2010) 118–123, https://doi.org/10.1016/j.jnucmat.2010.04.007.

[10] L.F. Johnson, H.J. Guggenheim, Infrared-pumped visible laser, Appl. Phys. Lett. 19 (2) (1971) 44–47, https://doi.org/10.1063/1.1653816.

[11] P. Egger, J. Hulliger, Optical materials for short wavelength generation, Coord. Chem. Rev. 183 (1) (1999) 101–115, https://doi.org/10.1016/S0010-8545(98)00101-5.

[12] V. Toccafondo, A. Cerqueira, S.S. Faralli, E. Sani, A. Toncelli, M. Tonelli, F. Di Pasquale, Er3+-doped BaY_2F_8 crystal waveguides for broadband optical amplification at 1.5μm, J. Appl. Phys. 101 (2) (2007), 023104, https://doi.org/10.1063/1.2404327.

[13] B.P. Sobolev, Multicomponent Crystals Based on Heavy Metal Fluorides for Radiation Detectors, Arxius de les Seccions de Ciències, Institut d'Estudis Catalans, 1994.

[14] J.C. Van 't Spijker, P. Dorenbos, C.W. Van Eijk, K. Krämer, H.U. Güdel, Scintillation and luminescence properties of Ce3+ doped K2LaCl5, J. Lumin. 85 (1–3) (1999) 1–10, https://doi.org/10.1016/S0022-2313(99)00170-2.

[15] A.C. De Mello, A.B. Andrade, G.H. Nakamura, S.L. Baldochi, M.E. Valerio, Scintillation mechanism of Tb3+ doped BaY2F 8, Opt. Mater. 32 (10) (2010) 1337–1340, https://doi.org/10.1016/j.optmat.2010.04.016.

[16] A.C. de Mello, A.B. Andrade, G.H. Nakamura, S.L. Baldochi, M.E. Valerio, Luminescence properties of Er3+ and Tm3+ doped BaY_2F_8, J. Lumin. 138 (2013) 19–24, https://doi.org/10.1016/j.jlumin.2012.12.001. https://linkinghub.elsevier.com/retrieve/pii/S0022231312007107.

[17] F. Auzel, Upconversion and anti-Stokes processes with f and d ions in solids, Chem. Rev. 104 (1) (2004) 139–174, https://doi.org/10.1021/cr020357g.

[18] A. Shalav, B.S. Richards, T. Trupke, K.W. Krämer, H.U. Güdel, Application of NaYF4: Er3+ up-converting phosphors for enhanced near-infrared silicon solar cell response, Appl. Phys. Lett. 86 (1) (2005) 86–88, https://doi.org/10.1063/1.1844592.

[19] T. Trupke, A. Shalav, B.S. Richards, P. Würfel, M.A. Green, Efficiency enhancement of solar cells by luminescent up-conversion of sunlight, Sol. Energy Mater. Sol. Cell. 90 (18–19) (2006) 3327–3338, https://doi.org/10.1016/j.solmat.2005.09.021.

[20] B.M. van der Ende, L. Aarts, A. Meijerink, Lanthanide ions as spectral converters for solar cells, Phys. Chem. Chem. Phys. 11 (47) (2009) 11081–11095, https://doi.org/10.1039/b913877c.

[21] S. Fischer, A. Ivaturi, B. Frohlich, M. Rudiger, A. Richter, K.W. Kramer, B. S. Richards, J.C. Goldschmidt, Upconverter silicon solar cell devices for efficient utilization of sub-band-gap photons under concentrated solar radiation, IEEE J. Photovoltaics 4 (1) (2014) 183–189, https://doi.org/10.1109/JPHOTOV.2013.2282744.

[22] F. Wang, D. Banerjee, Y. Liu, X. Chen, X. Liu, Upconversion nanoparticles in biological labeling, imaging, and therapy, Analyst 135 (8) (2010) 1839–1854, https://doi.org/10.1039/c0an00144a.

[23] Y.I. Park, K.T. Lee, Y.D. Suh, T. Hyeon, Upconverting nanoparticles: a versatile platform for wide-field two-photon microscopy and multi-modal in vivo imaging, Chem. Soc. Rev. 44 (6) (2015) 1302–1317, https://doi.org/10.1039/c4cs00173g.

[24] D.E. Dolmans, D. Fukumura, R.K. Jain, Photodynamic therapy for cancer, Nat. Rev. Canc. 3 (5) (2003) 380–387, https://doi.org/10.1038/nrc1071.

[25] F.C. Van Veggel, C. Dong, N.J. Johnson, J. Pichaandi, Ln3+-doped nanoparticles for upconversion and magnetic resonance imaging: some critical notes on recent progress and some aspects to be considered, Nanoscale 4 (23) (2012) 7309–7321, https://doi.org/10.1039/c2nr32124f.

[26] G. Chen, G. Han, Theranostic upconversion nanoparticles (I), Theranostics 3 (4) (2013) 289–291, https://doi.org/10.7150/thno.6382.

[27] R.M. Macfarlane, F. Tong, A.J. Silversmith, W. Lenth, Violet cw neodymium upconversion laser, Appl. Phys. Lett. 52 (16) (1988) 1300–1302, https://doi.org/10.1063/1.99681.

[28] A. Pandey, V.K. Rai, V. Kumar, V. Kumar, H.C. Swart, Upconversion based temperature sensing ability of Er3+-Yb3+codoped SrWO4: an optical heating phosphor, Sensor. Actuator. B Chem. 209 (2015) 352–358, https://doi.org/10.1016/j.snb.2014.11.126.

[29] H. Berthou, C. Jorgensen, Optical-fiber temperature sensor based on upconversion-excited fluorescence, Optic Lett. 15 (19) (1990) 1100–1102, https://doi.org/10.1364/OL.15.001100.

[30] F. Vetrone, R. Naccache, A. Zamarrón, A.J. De La Fuente, F. Sanz-Rodríguez, L. M. Maestro, E.M. Rodriguez, D. Jaque, J.G. Sole, J.A. Capobianco, Temperature sensing using fluorescent nanothermometers, ACS Nano 4 (6) (2010) 3254–3258, https://doi.org/10.1021/nn100244a.

[31] A. Shalav, B.S. Richards, M.A. Green, Luminescent layers for enhanced silicon solar cell performance: up-conversion, Sol. Energy Mater. Sol. Cell. 91 (9) (2007) 829–842, https://doi.org/10.1016/j.solmat.2007.02.007.

[32] B.S. Richards, A. Shalav, Enhancing the near-infrared spectral response of silicon optoelectronic devices via up-conversion, IEEE Trans. Electron. Dev. 54 (10) (2007) 2679–2684, https://doi.org/10.1109/TED.2007.903197.

[33] S. Fischer, J. C. Goldschmidt, P. Löper, G. H. Bauer, R. Brüggemann, K. Krämer, D. Biner, M. Hermle, S. W. Glunz, Enhancement of silicon solar cell efficiency by upconversion: optical and electrical characterization, J. Appl. Phys. 108 (4). doi: 10.1063/1.3478742.

[34] S.K.W. MacDougall, A. Ivaturi, J. Marques-Hueso, K.W. Krämer, B.S. Richards, Ultra-high photoluminescent quantum yield of upconversion for photovoltaic devices, Optic Express 20 (November) (2012) A879–A887, https://doi.org/10.1364/OE.20.00A879.

[35] A. Ivaturi, S. K. Macdougall, R. Martín-Rodríguez, M. Quintanilla, J. Marques-Hueso, K. W. Krämer, A. Meijerink, B. S. Richards, Optimizing infrared to near infrared upconversion quantum yield of β-NaYF4: Er3+ in fluoropolymer matrix for photovoltaic devices, J. Appl. Phys. 114 (1). doi:10.1063/1.4812578.

[36] R.E. Thoma, H. Insley, G.M. Hebert, The sodium fluoride-lanthanide trifluoride systems, Inorg. Chem. 5 (7) (1966) 1222–1229, https://doi.org/10.1021/ic50041a032.

[37] A. Boccolini, R. Faoro, E. Favilla, S. Veronesi, M. Tonelli, BaY_2F_8 doped with Er3+ : an upconverter material for photovoltaic application, J. Appl. Phys. 114 (6). doi: 10.1063/1.4817171.

[38] S. Fischer, E. Favilla, M. Tonelli, J.C. Goldschmidt, Record efficient upconverter solar cell devices with optimized bifacial silicon solar cells and monocrystalline BaY_2F_8:30% Er3+ upconverter, Sol. Energy Mater. Sol. Cell. 136 (2015) 127–134, https://doi.org/10.1016/j.solmat.2014.12.023.

[39] J.C. Goldschmidt, S. Fischer, B. Herter, B. Fröhlich, K.W. Krämer, B.S. Richards, A. Ivaturi, S.K. MacDougall, J. Marques Hueso, E. Favilla, M. Tonelli, Record efficient upconverter solar cell devices, in: 29th European PV Solar Energy Conference and Exhibition, Amsterdam, 2014, pp. 8–11.

[40] J.C. Goldschmidt, S. Fischer, Upconversion for photovoltaics - a review of materials, devices and concepts for performance enhancement, Adv. Opt. Mater. 3 (4) (2015) 510–535, https://doi.org/10.1002/adom.201500024.

[41] A. Rapaport, J. Milliez, M. Bass, A. Cassanho, H. Jenssen, Review of the properties of Up-conversion phosphors for new emissive displays, IEEE/OSA J. Disp. Technol. 2 (1) (2006) 68–78, https://doi.org/10.1109/JDT.2005.863781.

[42] C. Jones, N. Panov, A. Skripka, J. Gibbons, F. Hesse, J.-W. Bos, X. Wang, F. Vetrone, G. Chen, E. Hemmer, J. Marques Hueso, Effect of light scattering on upconversion photoluminescence quantum yield in microscale-to-nanoscale dispersions, Optic Express 28 (15) (2020) 22803–22818, https://doi.org/10.1364/oe.398353.

[43] F. Cornacchia, L. Palatella, A. Toncelli, M. Tonelli, A. Baraldi, R. Capelletti, E. Cavalli, K. Shimamura, T. Fukuda, Temperature dependence of impurity quenched luminescence in Tm3+:LiLuF4, J. Phys. Chem. Solid. 63 (2) (2002) 197–202, https://doi.org/10.1016/S0022-3697(01)00129-9.

[44] V.G. Badami, J. Liesener, C.J. Evans, P. De Groot, Evaluation of the measurement performance of a coherence scanning microscope using roughness specimens, in: Proceedings - ASPE 2011 Annual Meeting, vol. 52, 2011, pp. 23–26.

[45] J.M. Khosrofian, B.A. Garetz, Measurement of a Gaussian laser beam diameter through the direct inversion of knife-edge data, Appl. Optic. 22 (21) (1983) 3406, https://doi.org/10.1364/ao.22.003406.

[46] B. Cannon, T.S. Gardner, D.K. Cohen, Measurement of 1 um diameter beams, Appl. Optic. 25 (17) (1986) 2981–2983, https://doi.org/10.1364/AO.25.002981.

[47] K. Venkata Krishnaiah, G. Venkataiah, J. Marques-Hueso, P. Dharmaiah, C. K. Jayasankar, B.S. Richards, Broadband near-infrared luminescence and visible upconversion of Er 3+ -doped tungstate-tellurite glasses, Sci. Adv. Mater. 6 (xx) (2014) 1–9, https://doi.org/10.1166/sam.2015.2027.

[48] K. Venkata Krishnaiah, J. Marques-Hueso, K. Suresh, G. Venkataiah, B.S. Richards, C.K. Jayasankar, Spectroscopy and near infrared upconversion of Er3+-doped TZNT glasses, J. Lumin. 169 (2016) 270–276, https://doi.org/10.1016/j.jlumin.2015.08.035.

[49] J.A. Woollam, B.D. Johs, C.M. Herzinger, J.N. Hilfiker, R.A. Synowicki, C. L. Bungay, Overview of variable-angle spectroscopic ellipsometry (VASE): I. Basic theory and typical applications, in: SPIE 10294, Optical Metrology: A Critical Review, Denver, 1999, https://doi.org/10.1117/12.351660.

[50] B. Johs, J.A. Woollam, C.M. Herzinger, J.N. Hilfiker, R.A. Synowicki, C.L. Bungay, Overview of variable-angle spectroscopic ellipsometry (VASE): II. Advanced applications, in: SPIE 10294, Optical Metrology: A Critical Review, Denver, 1999, https://doi.org/10.1117/12.351667.

[51] H. Fujiwara, R.W. Collins (Eds.), Spectroscopic Ellipsometry for Photovoltaics - Volume 1: Fundamental Principles and Solar Cell Characterization, vol. 212, Springer International Publishing, 2018, https://doi.org/10.1007/978-3-319-95138-6.

[52] H.G. Tompkins, W.A. McGahan, Spectroscopic Ellipsometry and Reflectometry: A User's Guide, John Wiley & Sons, New York, 1999.

[53] M.E. Innocenzi, R.T. Swimm, M. Bass, R.H. French, M.R. Kokta, Optical absorption in undoped yttrium aluminum garnet, J. Appl. Phys. 68 (3) (1990) 1200–1204, https://doi.org/10.1063/1.346717.

[54] J.G. Liu, M. Ueda, High refractive index polymers: fundamental research and practical applications, J. Mater. Chem. 19 (47) (2009) 8907–8919, https://doi.org/10.1039/b909690f.

[55] N. Sultanova, S. Kasarova, I. Nikolov, Dispersion properties of optical polymers, Acta Phys. Pol., A 116 (2009) 585–587, https://doi.org/10.12693/APhysPolA.116.585. Belgrade.

[56] T. Higashihara, M. Ueda, Recent progress in high refractive index polymers, Macromolecules 48 (7) (2015) 1915–1929, https://doi.org/10.1021/ma502569r.

[57] J.D. Jackson, Classical Electrodynamics, third ed., Wiley, 2007.

[58] B.E.A. Saleh, M.C. Teich, Fundamentals of Photonics, second ed., John Wiley & Sons, 2007 https://doi.org/10.1002/0471213748 arXiv:0408133v1.

[59] J.F. Suyver, A. Aebischer, D. Biner, P. Gerner, J. Grimm, S. Heer, K.W. Krämer, C. Reinhard, H.U. Güdel, Novel materials doped with trivalent lanthanides and transition metal ions showing near-infrared to visible photon upconversion, Opt. Mater. 27 (6) (2005) 1111–1130, https://doi.org/10.1016/j.optmat.2004.10.021.

[60] A. Boccolini, E. Favilla, M. Tonelli, B.S. Richards, R.R. Thomson, Highly efficient upconversion in Er^3+ doped BaY_2F_8 single crystals: dependence of quantum yield on excitation wavelength and thickness, Optic Express 23 (15) (2015), https://doi.org/10.1364/OE.23.00A903. A903–A915.

[61] F. Zhang, Photon Upconversion Nanomaterials, first ed., vol. 3, Springer, Berlin, Heidelberg, 2015 https://doi.org/10.1007/978-3-662-45597-5.

[62] F.A. Jenkins, H.E. White, Fundamentals of Optics, forth ed., Tata McGraw-Hill Education, 1981.

[63] W. Sellmeier, Zur Erklärung der abnormen Farbenfolge im Spectrum einiger Substanzen, Annalen der Physik und Chemie (6) (2019) 272–282, https://doi.org/10.1002/andp.18712190612, 1871.

[64] K. Levenberg, F. Arsenal, A method for the solution of certain non-linear problems in least squares, Q. Appl. Math. 1 (278) (1943) 536–538, https://doi.org/10.1090/qam/10666.

[65] D.W. Marquardt, An algorithm for least-squares estimation of nonlinear parameters, J. Soc. Ind. Appl. Math. 11 (2) (1963) 431–441, https://doi.org/10.1137/0111030.
[66] J.W. Gooch, Cauchy's Dispersion Formula, Springer New York, New York, NY, 2007, p. 167, https://doi.org/10.1007/978-0-387-30160-0_2019.
[67] C.E. Webb, J.D.C. Jones (Eds.), Handbook of Laser Technology and Applications: Applications, Illustrate Edition, Handbook of Laser Technology and Applications, CRC Press, 2004.
[68] J. En Cai, L. Qiang, N. Ming Ming, L. Hui, H. Yu Xi, Z. G. Guan, M. L. Gong, Spectroscopic properties of heavily Ho3+ -doped barium yttrium fluoride crystals, Chin. Phys. B 24 (9). doi:10.1088/1674-1056/24/9/094216.
[69] M.J. Weber, CRC Handbook of Laser Science and Technology, CRC Handbook of Laser Science and Technology, CRC Press, 1987.
[70] A. Toncelli, F. Moglia, M. Tonelli, Optical properties of Eu2+ ions in BaY_2F_8 for completely-solid-state cw UV laser emission, Opt. Mater. 33 (1) (2010) 22–25, https://doi.org/10.1016/j.optmat.2010.07.009.
[71] P.E. Ciddor, Refractive index of air: new equations for the visible and near infrared, Appl. Optic. 35 (9) (1996) 1566, https://doi.org/10.1364/ao.35.001566.